Water Resources Management (2022) 36:315–339
https://doi.org/10.1007/s11269-021-03029-5

Calibration of METRIC Modeling for Evapotranspiration Estimation Using Landsat 8 Imagery Data

Masoud Derakhshandeh[1] · **Mustafa Tombul**[2]

Received: 6 April 2021 / Accepted: 9 November 2021 / Published online: 18 November 2021

Abstract
Water resources management needs efficient tools to estimate the rate of water loss through evapotranspiration (ET). High resolution spatial imagery has provided a valuable source of data which their implementation in well-tuned models has the potential of evapotranspiration rate estimations with satisfactory accuracy. Mapping evapotranspiration at high resolution with internalized calibration (METRIC) is basically an energy balance model which has shown a good performance in different applications. The model needs to be calibrated for various source of spatial data and with the introduction of new empirical correlations for numerous variables which are used in the model, the model is recalibrated for Landsat 8 multispectral image and applied to intensively cultivated agriculture lands in Alpu (Eskisehir, Turkey). In previous studies, the correlations from previous studies were referenced where the procedure was confusing for many users. In this work, a descriptive step by step procedure is also provided. The meteorological 24 h relative ET was then used to spread the instant ET (at image capture time) estimation into daily 24 h estimation. This approach reduces the errors from multiple correlations and to some extent the effect of short variations like partial cloud coverage.

Keywords METRIC method, Evapotranspiration · Energy balance · Land surface temperature · Landsat 8

1 Introduction

Evapotranspiration (ET) is a combined phenomenon of water loss through direct evaporation from ground surface and transpiration from vegetation (Paredes and Pereira 2019; Xiang et al. 2020). Estimation of ET rate is interested in agriculture monitoring and

✉ Masoud Derakhshandeh
mderakhshandeh@gelisim.edu.tr

Mustafa Tombul
mtombul@eskisehir.edu.tr

[1] Faculty of Engineering and Architecture, Civil Engineering Department, Istanbul Gelisim University, 34310 Istanbul, Turkey

[2] Civil Engineering Department, Eskişehir Technical University, Engineering Faculty, 26555 Eskisehir, Turkey

planning, water resource management, hydrology, meteorology and environmental studies (Xiang et al. 2020). While there are different methods with various principles (Zhao et al. 2013), the most common method for these estimations is an energy balance based on local meteorological data (Paredes and Pereira 2019; Xiang et al. 2020). Currently, the energy balance model known as Penman-Monteith is widely being used (Paredes and Pereira 2019) and documented as a standard method by FAO (Paredes and Pereira 2019). For applications in large area with different topographic and vegetation features, the classic methods show significant errors and fail to be applicable. Developments in the remote sensing techniques with high resolution multispectral bands enables us to even reach details of land surface and its covering.

Bastiaanssen (1995, 2000) introduced Surface Energy Balance Algorithm for Land (SEBAL) method which is based on the energy balance of radiation energy, ground latent heat and sensible heat transfer between land surface and nearby atmosphere using spatial data. The method successfully applied by many researchers (Li and Zhao 2010; Sun et al. 2011; Huang et al. 2021) using spatial data from different platforms including MODIS , Landsat TM5 (Li and Zhao 2010), Landsat 7 (Sun et al. 2011) and others. In SEBAL, the challenging part is the estimation of sensible heat flux (H) between surface and the atmosphere. This term can be estimated using an aerodynamic resistance dependent heat transfer equation (Bastiaanssen 2000; Li and Zhao 2010; Sun et al. 2011) which also requires temperature gradient between adjacent layer to the surface and another higher surface which are normally 0.1 m and 2.0 m height. This temperature gradient was assumed to be a linear function of surface temperature by Bastiaanssen (1995, 2000). This assumption removes the need for exact determination of surface temperature which is very challenging for many variable surface properties and radiometric calibrations of thermal sensors (Allen et al. 2007). Finding the coefficients of the linear equation requires the implementation of two point values which have known H values. In SEBAL, these two points are a wet pixel with assumed H value of zero and a dry pixel were ET is assumed to be zero and H equals the difference between net radiation and ground heat flux (Bastiaanssen et al. 1999; Bastiaanssen 2000). Since aerodynamic resistance depends on H value and vice versa, an internal calibration loop with some iteration converges to final estimations for H.

In an improving attempt by Allen et al. (2007), weather-based reference ET was used to determine energy balance conditions at wet/cold pixel. They called the method as "Mapping evapotranspiration at high resolution with internalized calibration" (METRIC) which is basically an improved version of SEBAL method. The details of the method are provided in following sections. The method was recalibrated for various sensors and applied over different land coverage and vegetation (Lian and Huang 2015; Madugundu et al. 2017; Baeumler et al. 2019; Ortega-Salazar et al. 2021).

Application of METRIC model based on high resolution (30 m) Landsat 8 imagery data in a region which has spatially diverse farming type were not tried elsewhere in a similar way. The approach also requires implementation of split window algorithm to obtain land surface temperature because of availability of two TIR bands on Landsat 8 platform. The work aimed to show that after calibrations, METRIC modelling can be used to obtain a reasonable estimation of ET over an area where its vegetation type changes considerably in small distances. The ability of METRIC to provide farm based estimations scrutinized in this way. This is very important for water management and planning in smaller scale.

While various studies reported the application of METRIC method, the details of calculations are not clear in many of them so that a new user would have serious problem to understand the steps and obtain information which needs to be reconsidered for a new application. In the present study, the method was applied over Alpu region in Eskişehir

district of Turkey which is an agriculture intensive area. A short description of implemented principles is also provided to provide better understanding of the procedure for new researchers in the field. The principal reference for the METRIC method which is also used in this study is the work of Allen et al. (2007). Modifications are applied to tune the procedure for Landsat 8 data.

2 Materials and Methods

The area of interest was Alpu region, Eskishehir district, Turkey (Fig. 1). The area is well-known for high productivity of agriculture product and very diverse type of vegetation. The calculations, visualization and mapping tasks were done using ArcGIS software package (ESRI).

For this study multi spectral images from Landsat 8 along with Digital Elevation Model (DEM) from Shuttle Radar Topography Mission (SRTM) SRTM was used (https://earthexplorer.usgs.gov/). The meteorological data was obtained from Turkey General Directorate of Meteorology.

2.1 Procedure

In METRIC, an energy balance is applied on an interested area to calculate the energy which is required for evaporation of water molecules. The method is actually an energy balance which uses remotely sensed data from different bands of a satellite imagery to calculate effective energy terms and finally relates ET to the residual of the surface energy balance (Eq. 1). It is a simple equation stating that the incoming energy through radiation will either be absorbed by ground (G), transferred to the surrounding atmosphere (H) or absorbed by water molecules as latent heat for evaporation (Fig. 2).

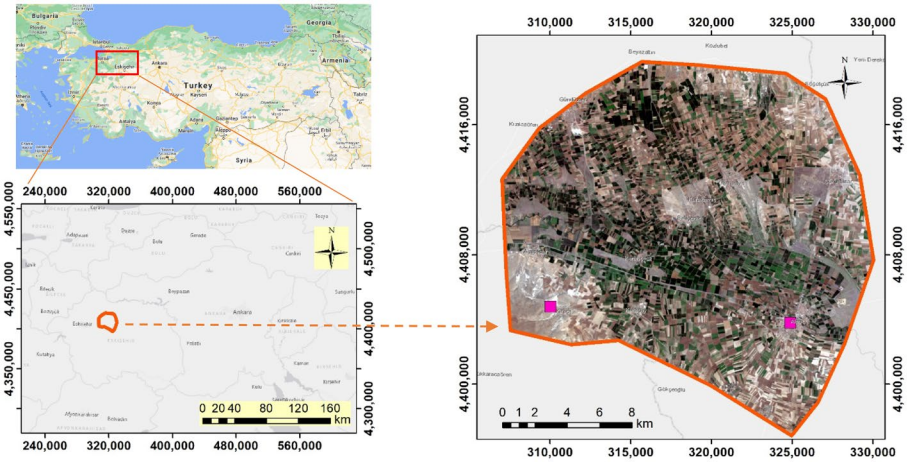

Fig. 1 Geographic location of study area Alpu, Eskişehir district of Turkey. Two purple squares are the location of meteorological stations

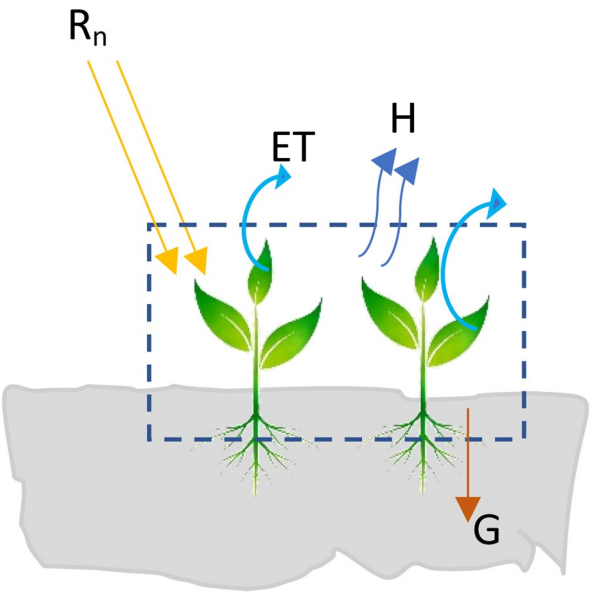

Fig. 2 The energy balance of ET based on other energy terms including net radiation (Rn), sensible heat flux to adjacent atmosphere (H) and the energy absorbed by the ground (G)

$$LE = R_n - G - H \tag{1}$$

where LE is the latent energy and driving force of ET, R_n is net radiation energy reaching surface (W/m^2), G is the energy transferred to ground (W/m^2) and H is the energy transferred to adjacent atmosphere known as sensible heat flux (W/m^2). In this equation minor energy terms like the energy required for photosynthesis and the changes in sensible heat of vegetation mass is ignored (Bastiaanssen 1995).

2.2 Estimation of Net Radiation Energy (R_n)

Planck's law describes the amount of energy ($W.m^{-2}.\mu m^{-1}$) released through electromagnetic waves from a black body at temperature T (K) at different wavelengths (Eq. 2).

The land surface is exposed to two main source of electromagnetic energy of sun and the surrounding environment or atmosphere. The nominal surface temperature of sun is about 6000 K and therefore according to the Planck's law (Eq. 2) and Wein's displacement law, the maximum radiation will be at 0.48 μm which is in shortwave range. Similarly for the nearby atmosphere or environment the temperature is around 300 K where the maximum energy is emitted at a long wave length of about 9.66 μm.

$$L_\lambda(T) = \frac{3.74 \times 10^8}{\lambda^5}\left[e^{\left(\frac{1.44\times10^4}{\lambda T}\right)} - 1\right]^{-1} \tag{2}$$

Net radiation R_n is calculated by subtracting leaving radiation from incoming radiation as shown in Fig. 2 The energy balance of ETis presented in Eq. (3). (Bastiaanssen 1995; Allen et al. 2007):

$$R_n = R_{si} - \alpha R_{si} + R_{Li} - R_{Lo} - (1 - \varepsilon_0) \times R_{Li} \quad (3)$$

In this equation, R_{Si} is the solar incoming short-wave radiation (W/m^2) where part of that is reflected by land surface proportional to surface albedo α which is a dimensionless coefficient; From surrounding atmosphere, the land surface receives long-wave radiation (W/m^2) R_{Li} which also part of that is reflected proportional to land surface reflectivity (1- ε_o). Here, ε_o is the emissivity of the land surface over broad-band range. The land surface also emits radiation R_{Lo} at longwave range.

The details of calculations for all coefficients and factors are presented below.

2.2.1 Surface Albedo

Surface albedo, is the property of surface which quantifies the reflectivity of surface in short-wave range. It is the ratio of reflected solar radiation to the incident solar short-wave radiation at the surface. It is not solely a surface property dependent factor where it also changes by the spectrum and the angular properties of the solar radiation. A surface with high albedo like a snow cover reflects most of incident radiation while a low albedo surface like a heavy forestry area absorbs the majority of received radiation. The albedo is reported in the range of 0 to 1. It is said that uncertainties in albedo estimations is a significant source of error in climate studies (Liang 2001). Liang et al. (1999) has separated inherent albedo and apparent albedo where the former, at a given solar zenith angle and for a definite wavelength is an integration of bidirectional reflectance factor over the whole viewing angles which is independent from atmosphere condition. In contrast, the apparent albedo is the ratio of upwelling irradiance to downward irradiance for a given solar zenith angle and for a definite wavelength which is equivalent to what is measured using albedo meters on the field. Here the attempt is to calculate surface broadband albedo from narrowband multispectral sensors data at Top of Atmosphere (TOA).

For albedo calculation, digital numbers for each pixel of a Landsat image must be converted to Top of Atmosphere (TOA) reflectance. Liang (2001) introduced satellite specific algorithms to estimate albedo. Below formula is normalized version of Liang's formula for Landsat (Smith 2010);

$$\alpha_{short} = \frac{0.356\rho_1 + 0.130\rho_3 + 0.373\rho_4 + 0.085\rho_5 + 0.072\rho_7 - 0.0018}{0.365 + 0.130 + 0.373 + 0.085 + 0.072} \quad (4)$$

where ρ represents reflectance on top of atmosphere calculated from Landsat 7 bands 1,3,4,5, and 7. Correspondingly, for Landsat 8: 2,4,5,6 and 7 bands (Table 1) must be used.

Table 1 Landsat 7 and Landsat 8 bands used for albedo estimation

LandSAT 7		**LandSAT 8**	
B1 Blue	0.45 - 0.52 µm	B2 Blue	0.450 to 0.515 µm
B3 RED	0.63 - 0.69 µm	B4 RED	0.630 to 0.680 µm
B4 NIR	0.77 - 0.90 µm	B5 NIR	0.845 to 0.885 µm
B5 NIR	1.55 - 1.75 µm	B6 SWNIR	1.56 to 1.66 µm
B7 MIR	2.08 - 2.35 µm	B7 SWNIR	2.10 to 2.30 µm

Table 2 Split-window coefficients from (Madugundu et al. 2017) which is based on (Sobrino et al. 2003)

Split-window coefficients	value
C_0	-0.268
C_1	1.378
C_2	0.183
C_3	54.300
C_4	-2.238
C_5	-129.200
C_6	16.400

2.2.2 Conversion of Spectral Data to TOA Reflectance

TOA reflectance values can be calculated from reflective band DN's values using rescaling coefficients in the Meta Data file of Landsat 8 products using below equation:

$$\rho_{\lambda'} = M_\rho Q_{cal} + A_\rho \tag{5}$$

where in this formula; $\rho_{\lambda'}$ is TOA planetary reflectance, without correction for solar angle. M_ρ is band-specific multiplicative rescaling factor, A_ρ is band-specific additive rescaling factor and Q_{cal} is quantized and calibrated standard product pixel values (DN). All these coefficients are provided in metadata file of the image product. To apply correction for the solar angle:

$$\rho_\lambda = \rho_{\lambda'} / \sin(\theta_{SE}) \tag{6}$$

where, ρ_λ is TOA planetary reflectance and θ_{SE} is local sun elevation angle. The scene center sun elevation angle in degrees is provided in the metadata (SUN_ELEVATION). It was 65.3887 degree for the acquisition time of obtained image.

2.2.3 Broad-band surface emissivity (ε_o)

The estimation of land surface emissivity from remotely sensed spatial data is problematic mainly because this surface property also depends on the land surface temperature and vice versa. Additionally, the atmospheric situation is also another complicating factor where the emitted radiation from surface attenuates during its path to the sensors. A very good summary regarding the previous attempts for estimation of surface emissivity and its complexity is provided in (Li et al. 2013). In the present work, surface emissivity (ε_o) is estimated based on the empirical formula presented by Tasumi (2004). This is a function of leaf area index (LAI) which depends on Soil Adjusted Vegetative Index (SAVI).

$$\begin{aligned} \varepsilon_0 &= 0.95 + 0.01LAI \quad when\ LAI \leq 3 \\ \varepsilon_0 &= 0.98 \qquad\qquad when\ LAI > 3 \end{aligned} \tag{7}$$

where, Leaf Area Index (LAI) ($m^2\ m^{-2}$) is defined as the ratio of the total one side leaf area of leaves per unit of horizontal land surface area. LAI is an indicator of canopy foliage content and also provides a measure of resistance to vaporization. The empirical equation suggested by Bastiaanssen is used to calculate LAI (Bastiaanssen 2000).

$$LAI = -\frac{ln\left[\left(0.69 - SAVI_{ID}\right)/0.59\right]}{0.91} \tag{8}$$

SAVI index is estimated using the top of atmosphere reflectance values of the RED and NIR bands. For Landsat 8 images, the relation is given below (Huete 1988);

$$\text{SAVI} = \frac{(1+\text{L})(\rho_{t,5} - \rho_{t,4})}{\text{L} + (\rho_{t,5} + \rho_{t,4})} \tag{9}$$

where, L is a constant and as was suggested by Allen et al. (2007) we use L=0.1 to minimize soil background biases. In METRIC, LAI is limited to 6.0 when $\text{SAVI}_{ID} > 0.687$ and LAI=0 when $\text{SAVI}_{ID} < 0.1$. There are many sources of uncertainty in determination of LAI, but the impact of those errors are not significant in energy balance (Allen et al. 2007).

2.3 Incoming Solar Radiation

This is the main source of energy for ET and reaches the Earth's surface (W/m^2) through direct or diffuse radiation. It is computed from solar constant radiation energy per unit area and corrected for various solar incidence angle, atmospheric transmissivity and relative Earth–Sun distance.

$$RS_i = \frac{G_{sc}\cos\theta_{rel}\tau_{sw}}{d^2} \tag{10}$$

Here, G_{sc} is solar constant equal to1367 (W/m^2); θ_{rel} is the solar incidence angle; d^2 is the square of the relative earth–sun distance; and τ_{sw} is broad-band atmospheric transmissivity. For θ_{rel} then;

$$\begin{aligned}\cos\theta_{rel} = {} & \sin(\delta)\sin(\varphi)\cos(s) - \sin(\delta)\cos(\varphi)\sin(s)\cos(\gamma) + \cos(\delta)\cos(\varphi)\cos(s)\cos(\omega) \\ & + \cos(\delta)\sin(\varphi)\sin(s)\cos(\gamma)\cos(\omega) + \cos(\delta)\sin(\gamma)\sin(s)\sin(\omega)\end{aligned} \tag{11}$$

where δ is declination of the Earth (Eq. 12) and d is the day of the year which in this work was day 182 (01.07.2019) and δ equals to 23.12 degree.

$$\delta = 23.45^o \times \sin\left(\frac{360}{365} \times (d + 284)\right) \tag{12}$$

ϕ is the latitude coordinate of each pixel which does not change too much over a small area.

Parameter ω is the hour angle (Eq. 13), specifying the solar position on the sky. It equals to 0 at solar noon, takes a negative value in morning and becomes positive in afternoon. The hour angle was calculated equal to -52.5 degree at scene center time.

$$\omega = 15 \times (local\ time - 12) \tag{13}$$

Parameter s is surface slope where s is zero for horizontal surface and equals to π/2 radians for vertical surface and always positive between these two limits for other inclinations. DEM data is required to calculate slope. The obtained multiple DEM data was combined to fully cover the Landsat image.

Parameter γ is the surface aspect angle, where for surfaces faced south equals zero, for east faced surface equals –π/2, for west faced surface equals + π /2 and for slopes faced north γ = ± π radians. The surface aspect angle was calculated using "Aspect tool" in ArcGIS.

τ_{sw} is estimated as a function of atmospheric pressure P (kPa), water content in the atmosphere W (mm) and solar zenith angle over a horizontal surface θ_{hor} , using an empirical formula from ASCE-EWRI (Walter et al. 2000) ;

$$\tau_{sw} = 0.35 + 0.627exp\left[\frac{-0{,}00146P}{K_t cos\theta_{hor}} - 0.075(\frac{W}{cos\theta_{hor}})^{0.4}\right] \tag{14}$$

The parameter K_t is a unitless turbidity coefficient $0<K_t<1.0$, where K_t equals one for clean air and 0.5 for extremely turbid, dusty, or polluted air. $P/(\cos\theta_{hor})$ is a surrogate for atmospheric mass and optical path length.

P (kPa), is calculated by ASCE-EWRI 2005 as;

$$P = 101.3\left(\frac{293 - 0.0065z}{293}\right)^{5.26} \tag{15}$$

where, z (m) is the elevation for each pixel and was obtained from DEM.

Water content of atmosphere is calculated from (Garrison and Adler 1990);

$$w_{est} = 0.14e_o\left(\frac{P_o}{P_{oo}}\right) + 0.21(\text{cm}) \tag{16}$$

$$e_o = he_s \tag{17}$$

$$log_{10}e_s = 8.42926609 - \frac{1827.17843}{T} - \frac{71208.271}{T^2} \tag{18}$$

h is the relative humidity at acquisition time which was 55%. The temperature (T) was 290.36 K.

e_s is saturated vapor pressure and was 19.58 mbar. Therefore, e_o was calculated 10.77 mbar. P_{oo} at sea level was 101.325 kpa.

In the Eq. (14), the term cos θ_{hor} is;

$$\cos\theta_{hor} = \sin(\delta)\sin(\varphi) + \cos(\delta)\cos(\varphi)\cos(\omega) \tag{19}$$

Parameter d^2 in Eq. (10) is the square of earth-sun distance and can be calculated as a function of the day of the year DOY:

$$d^2 = \frac{1}{1 + 0.033\cos(DOY\frac{2\pi}{365})} \tag{20}$$

2.4 Outgoing Long-wave Radiation

Outgoing long-wave radiation (RL_o) from the surface is a function of land surface temperature and also surface emissivity which can be calculated from the Stefan–Boltzmann equation:

$$RL_o = \varepsilon_0 \sigma T_s^4 \tag{21}$$

where ε_0 is broad-band surface emissivity dimensionless as provided in Eq. (7); σ is Stefan–Boltzmann constant 5.67×10^{-8} $W.m^{-2}.K^{-4}$, and T_s is the Land Surface Temperature (LST) K and must be estimated from spatial data.

Land surface temperature was calculated using below equation (Eq. 22) (Madugundu et al. 2017) which is a split window algorithm. A split window algorithm must be used for LST estimation using Landsat 8 data because there are to thermal infra-red bands including bands10 and 11on this platform. The coefficients C_0 to C_6 are provided in Table 2.

$$LST = TB_{10} + C_1\left(TB_{10} - TB_{11}\right) + C_2(TB_{10} - TB_{11})^2$$

$$+C_0 + \left(C_3 + C_4 W\right)(1-\varepsilon) + (C_5 + C_6 W)\Delta\varepsilon \tag{22}$$

For Landsat 8 in analogy with MODIS (Sobrino et al. 2003) following equations are applicable:

$$\varepsilon = \frac{\left(LSE_{10} + LSE_{11}\right)}{2} \tag{23}$$

$$\Delta\varepsilon = LSE_{10} - LSE_{11} \tag{24}$$

LSE for 0<FVC<1 :

$$LSE = \varepsilon_s(1 - FVC) + \varepsilon_v.FVC \tag{25}$$

$$FVC = \frac{NDVI - NDVI_s}{NDVI_v - NDVI_s} \tag{26}$$

$$NDVI = \frac{B_5 - B_4}{B_5 + B_4} \text{ for Landsat 8 bands} \tag{27}$$

NDVIs is soil NDVI which is better to be determined statistically based on the scene NDVI for bare soil pixels but here we calculated average of 10 points NDVI value for soil pixels and calculated equal to 0.17.

The NDVIv index is also similar to the NDVIs but the former is for vegetation pixels. It is calculated as the maximum NDVI value of the scene which was 0.6707.

Band 10 and 11 emissivity values (Table 3) for vegetation and soil are different and was obtained from other references (Jin et al. 2015; Madugundu et al. 2017). Similar

Table 3 Thermal Infra-Red emissivity for soil and vegetation

Landsat 8 TIRS	Thermal constants		Rescaling factors		Emissivity values	
	K_1	K_2	M_L	A_L	ε_s	ε_v
Band 10	1321.08	777.89	0.000342	0.1	0.971	0.987
Band 11	1201.14	480.89	0.000342	0.1	0.977	0.989

works have taken this values from ECOSTRESS Spectral Library available on (https://speclib.jpl.nasa.gov/).

T_B (K) in Eq. (22) is the Top of atmosphere brightness temperature, and is calculated using:

$$T = \frac{K_2}{ln(\frac{K_1}{L_\lambda} + 1)} \tag{28}$$

where L_λ is TOA spectral radiance (W. m^{-2}.$srad^{-1}$.μm^{-1}), is calculated as:

$$\boldsymbol{L_\lambda = M_L Q_{cal} + A_L} \tag{29}$$

where M_L is band-specific multiplicative rescaling factor; A_L is band-specific additive rescaling factor; and Q_{cal} is quantized and calibrated standard product pixel values (DN). These are provided as metadata of the image product.

In Eq. (28), K_1 is band-specific thermal conversion constant; K_2 is band-specific thermal conversion constant. They are also obtained from metadata.

In the Eq. (22), W is the water content to be calculated in gr.cm^{-2}. Here, water content is the amount of water in a vertical column of atmosphere over 1 cm^2 area. The calculated water content must be in cm of liquid water which actually means the amount of condensed water in a container with the same cross-sectional area of the column. Therefore, by assuming a liquid water density equal to 1 gr.cm^{-3}, the result of Eq. (16) can be directly used for LST calculation in Eq. (19).

2.5 Incoming Long-wave Radiation

The atmosphere above the land surface emits radiation mainly in longwave range, because of its moderate temperature. Again Boltzmann equation can be used to estimate this incoming energy. Since this radiation is being emitted from a thin layer of nearby atmosphere, the temperature used in the equation must be an estimated near surface air temperature.

$$RL_i = \varepsilon_a \sigma T_a^4 \tag{30}$$

where ε_a is the effective atmospheric emissivity (Eq. 31), and T_a is near-surface air temperature K.

$$\varepsilon_a = 0.85(-\ln\tau_{sw})^{0.09} \tag{31}$$

Table 4 The estimated incoming radiation energy, ground and sensible heat values at hot and cold pixels

Pixel	Coord.	Rn	G	LE	H
Hot	30°58'8.669"E 39°50'32.806"N	221.9	62.23	0	158.77
Cold	30°50'45.584"E 39°52'50.046"N	392.0	46.8	329.6	15.6

Here, τ_{sw} = broad-band atmospheric transmissivity for shortwave radiation calculated from Eq. (14).

The near surface temperature was estimated using local air temperature data and corrected for elevation using a lapse rate coefficient of 6.49 K.km^{-1} (Sissenwine et al. 1962). Local temperature was (Eskisehir 01.07.2019) 290.16 K .

2.6 Soil Heat Flux (G) Estimation

Soil heat flux is a measure of the amount of energy being absorbed and stored by soil and is generally reported as the rate of energy per unit area and time (W.m^{-2}). The land vegetation coverage or closure is the determining factor where generally two empirical relations for a dense coverage and/or sparse coverage are introduced in the literature. Besides, the amount of energy which can be stored in the soil, depends on the net amount of energy which reaches to the surface. Therefore, soil heat flux is always a fraction of total net radiation R_n in METRIC applications (Tasumi 2004).

$$\frac{G}{R_n} = 0.05 + 0.18e^{-0.521LAI}(LAI \geq 0.5) \tag{32}$$

$$\frac{G}{R_n} = 1.80\frac{(T_s - 273.15)}{R_n} + 0.084(LAI < 0.5) \tag{33}$$

2.7 Sensible Heat Flux (H) Estimation

Sensible heat flux is the amount of energy being convected from land surface to the atmosphere which physically happens when land surface temperature is higher than the adjacent air layer. While this is the driving force, an aerodynamic resistance factor determines the rate of the energy transfer. This is similar to Ohm's resistance formula for any transport between to reference points. In METRIC, a one-dimensional aerodynamic function is used to estimate H as schematically shown in Fig. 3:

$$H = \rho \times c_p \times \frac{dT}{r_{ah}} = \rho \times c_p \times \frac{T_s - T_a}{r_{ah}} \tag{34}$$

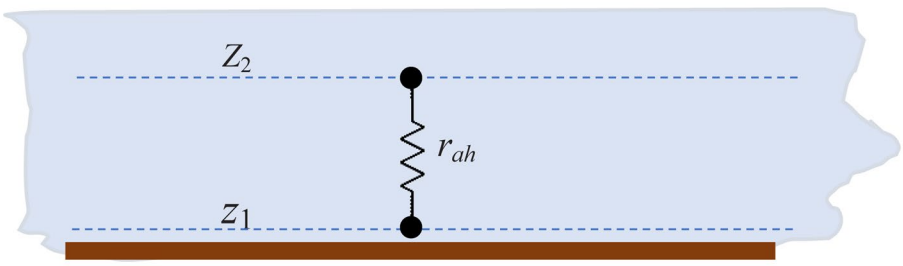

Fig. 3 Sensible heat transfer calculation using aerodynamic resistance at two near surface elevations. This is similar to Ohm's resistance formula for any transport between to reference points

where, ρ_{air} is air density (kg.m^{-3}); C_p is the specific heat of air at constant pressure (J.kg^{-1}.K^{-1}) and assumed constant (1005 j.kg^{-1}.K^{-1}); and r_{ah} (Eq. 45) is aerodynamic resistance (s.m^{-1}) which decreases substantially with the increase of wind speed and turbulences in the surrounding atmosphere. In Eq. (1), horizontal convection of heat is ignored, which means the governing heat transfer is being transferred just vertically. This is physically acceptable when the resistance between two near layer over the land surface is considered. In METRIC they are assumed as 0.1 and 2 m above the surface. These are computed as a function of estimated aerodynamic roughness of the particular pixel (Bastiaanssen 2000; Allen et al. 2007).

The Air density can be calculated using below equation:

$$\rho = \frac{1000P}{1.01(T_s - \delta T)R} \tag{35}$$

where P is mean atmospheric pressure at each specific pixel elevation (kPa) and estimated for each pixel using Eq. (15). R is universal ideal gas constant (287 J.kg^{-1}.K^{-1}); and T_s-δT is surrogate near-surface air temperature (K). The δT in surrogate temperature can be estimated using measured air temperature data from nearby stations and LST at that pixel. For the date of image, the Alpu station air temperature was recorded as 21.5 °C. The LST for that point on the LST map was obtained as 312.6 K. Therefore:

$$\delta T_1 = 312.6 - (21.5 + 273.16) = 17.94$$

with the same procedure for Kireçköy station:

$$\delta T_2 = 312.4 - (19.5 + 273.16) = 19.74$$

The average of these two values where considered for other pixels to estimate near surface air temperature over the scene related to LST.

The dT parameter (K) in Eq. (34) is the best approximation for the near surface temperature difference at z_1 and z_2 heights. Since the surface properties and consequently LST is not the same over the scene, dT is defined to be floating throughout the scene, beyond the height for sensible heat roughness (z_{oh}) and zero plane displacement. Bastiaanssen (1995) showed that a linear relation between dT and the surface temperature (T_s) can well satisfy the required accuracy in ET estimations where he suggested the following relation.

$$dT = a + bT_{sdatum} \tag{36}$$

In this equation, a and b constants should be calculated for the acquired satellite image. T_{sdatum} is surface temperature recalculated for each pixel based on that pixel elevation from a digital elevation model and a customized lapse rate (L_R) (Eq. 37).

$$T_{s\,datum} = T_s - T_s \times DEM \tag{37}$$

T_{sdatum} for each pixel was produced using the LST and DEM data for near Alpu station (312.16 K, 764 m, with a dry adiabatic lapse rate: 9.8 °C.km^{-1}).

In METRIC we need to specify a cold and a hot pixel on the scene to find a and b constants. The pixel is considered “hot pixel” in the image where the soil is assumed to be completely dried so that there is no evapotranspiration (i.e. LE is zero), therefore (Allen et al. 2007);

$$H_{hot} = (R_n - G)_{hot} - LE_{hot} \tag{38}$$

$$dT_{hot} = \frac{(R_n - G)_{r_{ahhot}}}{\rho_{airhot} C_p} \tag{39}$$

where $r_{ah\ hot}$ is r_{ah} when computed for the roughness and stability conditions of the hot pixel, and ρ_{airhot} is the air density of the hot pixel as calculated in Eq. (35). On the other hand for the cold pixel where the ET is considerably high (Allen et al. 2007):

$$H_{cold} = (R_n - G)_{cold} - LE_{cold} \tag{40}$$

where, LE_{cold} is the estimated latent heat flux at the cold pixel. This can be provided from the estimated alfalfa reference crop ET_r . Reliable experiences showed that for a pixel in the image which contains the coldest and wettest vegetation cover with full cover LAI > 4 , the ET rates are typically about 5% higher than the rate from the alfalfa reference crop ET_r (Allen et al. 2007). The ET_r was recorded for Kireçköy station equal to 0.5 $mm.h^{-1}$ at the image acquisition time. From the following equation which is an energy balance for water evaporation, LE_{cold} can be calculated (Allen et al. 2007).

$$LE_{cold} = \frac{1.05 \times ET_r \times \lambda.\rho_w}{3.6 \times 10^6} \tag{41}$$

where λ is water latent heat of vaporization ($J.kg^{-1}$) and is computed as:

$$\lambda = \left[2.501 - 0.00236\left(T_s - 273.15\right)\right] \times 10^6 \tag{42}$$

ET_r ($mm.hr^{-1}$) is obtained from local station data, ρ is water density 1000 $kg.m^{-3}$. Therefore LE_{cold} was calculated equal to 329.6 $W.m^{-2}$.

$$dT_{cold} = \frac{(R_n - G - LE_{cold})_{r_{ahcold}}}{\rho_{air\ cold} C_p} \tag{43}$$

The obtained values for hot and cold pixels are provided in Table 4.

Still, the values for aerodynamic transport resistance r_{ah} at both hot and cold pixels must be determined to calculate dT values.

2.7.1 Aerodynamic Transport

The higher rate of sensible heat flux affects the buoyancy inside the boundary layer and the aerodynamic resistance ($r_{ah)}$ will decrease. At neutral stability condition, it is calculated using following equation (Allen et al. 2007):

$$r_{ah} = \frac{\ln(\frac{z_2}{z_1})}{u_* k} \tag{44}$$

Friction velocity u_* is estimated by obtaining logarithmic wind profile for presumed neutral atmospheric conditions:

$$u_* = \frac{\mathrm{k}u_{200}}{\ln(\frac{200}{z_{om}})} \tag{45}$$

where in this equation, u_{200} is wind speed (m.s^{-1}) at 200 m blending height, z_{om} is the roughness length for momentum (m), an effective factor in land-atmosphere energy exchange influencing turbulences. In the equation, the u_{200} wind speed is considered constant because at that height the wind profile is not affected by surface roughness but friction velocity u_* is changing for each pixel and calculated using specific roughness length for each pixel. The wind speed at 200 m blending height is estimated using (Allen et al. 2007):

$$u_{200} = \frac{u_w \ln(\frac{200}{z_{omw}})}{\ln(\frac{z_x}{z_{omw}})} \tag{46}$$

where u_w is wind speed from a nearby weather station and z_x is the weather station wind speed measurement height above the surface. z_{omw} is the roughness length for the weather station surface to be calculated using following equation (Faivre et al. 2017).

$$z_{0m} = 0.5 \times h \times \lambda_f \tag{47}$$

where h is an effective averaged obstacle height, and λ_f is the frontal area index defined as a proportion of frontal area A_f (perpendicular to the flow) to the total area covered by roughness elements A_T :

$$\lambda_f = \frac{A_f}{A_T} \tag{48}$$

For estimation of roughness length for momentum empirical equations are used where for agricultural areas, z_{om} is related to the LAI index.

Following correlation for agricultural crops less than about 1 m height was used (Tasumi 2004).

$$z_{0m} = 0.018\ LAI \tag{49}$$

There are other empirical alternatives of above equation for the estimation of z_{om} which uses NDVI and albedo as input factors (Allen et al. 2007). Also for applications in larger scale which may include mountainous areas, modified equations for u_{200} should be used to correct for that pixel elevation (Allen et al. 2007).

For hot and cold pixels, u_* was first calculated for neutral condition using Eq. (45). The u_{200} parameter was estimated using meteorology data and Eq. (46).

2.7.2 Stability Condition Correction Factors

The value for u_* was used to calculate Monin–Obukhov length *L to* define the stability conditions (Allen et al. 2007).

$$L = -\frac{\rho_{air} c_p u_*^3 T_s}{kgH} \tag{50}$$

The correction factors for heat and momentum transfer was then estimated using Eqs. (51)−(59) (Allen et al. 2007).

$$\Psi_{m(200\ m)} = 2\ln\left(\frac{1 + x_{(200\ m)}}{2}\right) + \ln\left(\frac{1 + x^2_{(200\ m)}}{2}\right) - 2\arctan\left(x_{(200\ m)}\right) + 0.5\pi \tag{51}$$

$$\Psi_{h(2\ m)} = 2\ln\left(\frac{1 + x^2_{(2\ m)}}{2}\right) \tag{52}$$

$$\Psi_{h(0.1\ m)} = 2\ln\left(\frac{1 + x^2_{(0{,}1\ m)}}{2}\right) \tag{53}$$

where;

$$x_{(200\ m)} = (1 - 16\frac{200}{L})^{0.25} \tag{54}$$

$$x_{(2\ m)} = (1 - 16\frac{2}{L})^{0.25} \tag{55}$$

$$x_{(0.1\ m)} = (1 - 16\frac{0.1}{L})^{0.25} \tag{56}$$

Values for $x_{200\ \mathrm{m}}$, $x_{2\ \mathrm{m}}$, and $x_{0.1\ \mathrm{m}}$ have no meaning when $L \geq 0$ and their values are set to 1.0. For $L > 0$ stable conditions (Allen et al. 2007):

$$\Psi_{m(200\ m)} = -5(\frac{200}{L}) \tag{57}$$

$$\Psi_{m(2\ m)} = -5(\frac{2}{L}) \tag{58}$$

$$\Psi_{m(0.1\ m)} = -5(\frac{0.1}{L}) \tag{59}$$

These factors was used to estimate new u_* for hot and cold pixels using Eq. (60).

$$u_* = \frac{\mathrm{k}u_{200}}{\ln\left(\frac{200}{z_{om}}\right) - \Psi_{m(200\ m)}} \tag{60}$$

Then using Eq. (61), r_{ah} was estimated for hot and cold pixels.

$$r_{ah} = \frac{\ln\left(\frac{z_2}{z_1}\right) - \Psi_{h(z_2)} + \Psi_{h(z_1)}}{u_* k} \tag{61}$$

Finally Eqs. (39) and (41) was used to determine dT_{hot} and dT_{cold} constants. These two values were used to find a and b values using Eq. (36).

2.7.3 Iterations for H and r_{ah} calibration

The values of dT for all pixels was determined using Eq. (36). The first iterative value for H was estimated using Eq. (34) for all pixels. This value was used to estimate Monin–Obukhov length L to define stability weight factors of all pixels over the scene. The correction factors for heat and momentum was used to calculate second iterative u^* using Eq. (60). Second iterative r_{ah} was calculated using Eq. (61). Then the new iterative H was calculated. This iteration cycle was repeated until the change between two consecutive iteration for H all over the scene was insignificant. In this study a good convergence was observed after 6 iterations.

2.8 Calculation of Evapotranspiration

ET flux can be calculated using a simple energy balance which is needed for water evaporization. The estimated value is for the instant time of image capture. For each pixel, dividing *LE (W/m²)* from Eq. (1) to the latent heat of vaporization of water will give the rate of ET:

$$ET_{inst} = 3.6 \times 10^6 \frac{LE}{\lambda \rho_w} \tag{62}$$

where, ET_{inst} is the instantaneous ET ($mm.h^{-1}$) ; The coefficient 3.6×10^6, converts from seconds to hours and meters to millimeters, ρ_w is liquid water density; and λ_w is latent heat of vaporization ($j.kg^{-1}$) for water.

To estimate the ET rate at other times of the day where the imagery data is not available, the ratio of the ET_{inst} to the reference ET_r data obtained from local meteorological stations is used. In METRIC, it is assumed that this reference ET fraction (ET_rF) is almost constant during 24 h;

$$ET_rF = \frac{ET_{inst}}{ET_r} \tag{63}$$

Finally, this fraction along with the summation of hourly records for relative evapotranspiration from meteorological data can be used to estimate satellite based estimation for the 24 hour evapotranspiration, ET_{24} (mm/day), for each image pixel as;

$$ET_{24} = ET_rF.ET_{r\_24} \tag{64}$$

where, the ET_{r_24} is the summation of hourly records for relative evapotranspiration from meteorological data.

3 Results and discussion

3.1 Evaluation of Main Parameters

The result for Albedo calculations is shown in Fig. 4. The albedo value for the selected area with weather and atmospheric condition at the acquisition day falls near zero for a low reflective coverage like water body, whereas it takes a value as high as 0.8 for highly reflective surfaces like bare soil.

The calculated LST was then mapped for the study area as shown in Fig. 5. It is clear that the LST for bare non irrigated land is significantly high. The estimated high 330 K temperatures belongs to those kind of land surface. The split window algorithm was successful in providing LST map with high sensitivity which is observed from the image as well.

The produced map for net radiation is presented in Fig. 6. On the map, adjacent farms are not distinguishable anymore which means during the summation of radiation

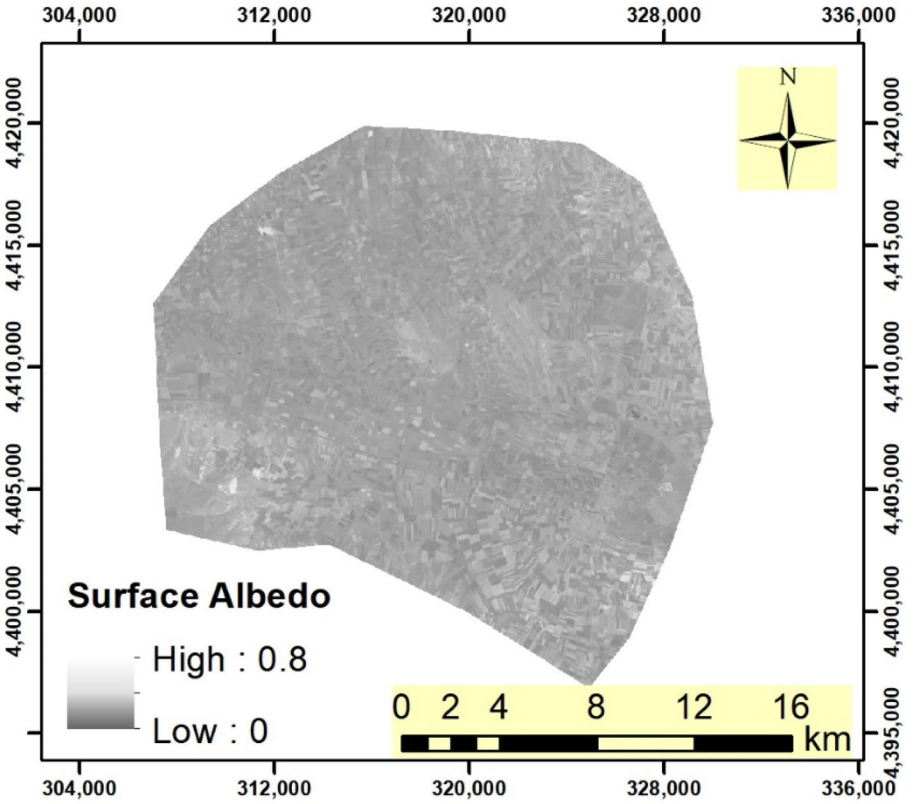

Fig. 4 The result for Albedo over the study area; Bright cells on the image represents higher albedo (i. e. high surface reflectance)

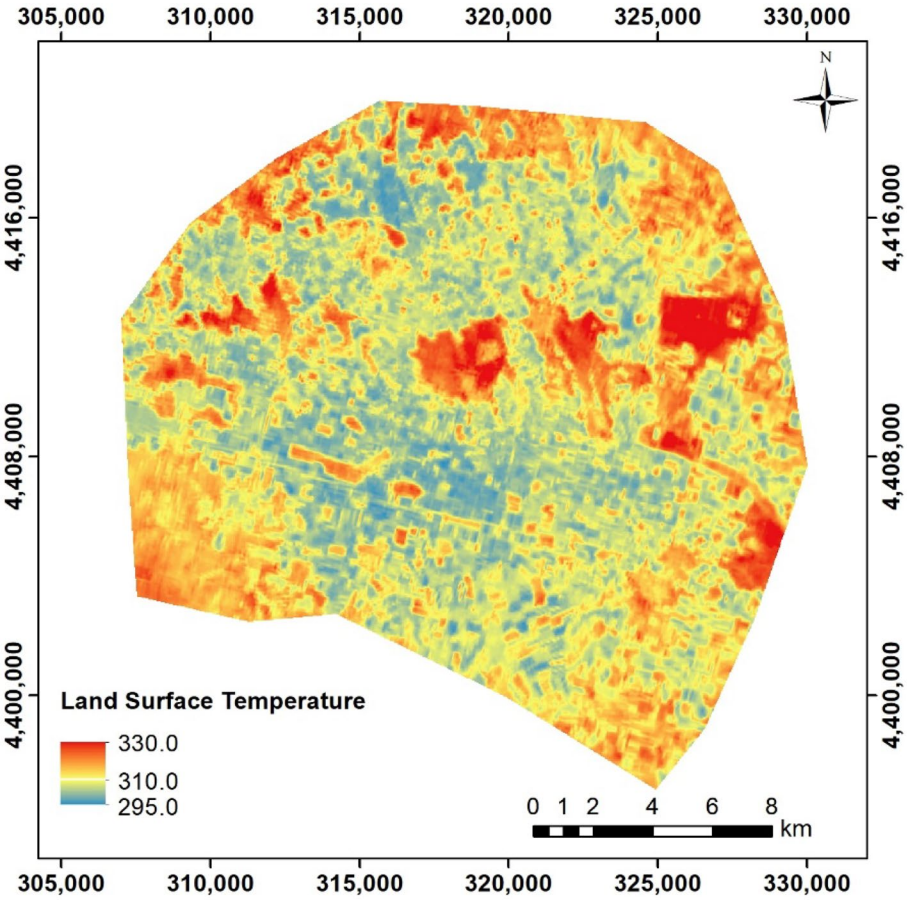

Fig. 5 Map of Land Surface Temperature (K) calculated using TIR bands (10 and 11) of Landsat 8 with a split window algorithm

terms, the energy term or terms which were less dependent on the vegetation pattern, type or quality were the determining term. Further discussions below explains this effect.

The final value for sensible heat flux is shown in Fig. 7. It is clear that METRIC model with applied six iterations for determining H, was successful in providing data which are sensitive to variations in small scale farms. The area without considerable vegetation like bared hills and residential area showed the lowest H value.

The finally obtained map of ET over the study area is shown in Fig. 8a. This is the estimated ET for the time of acquisition of the satellite image. For the current study the acquisition time was 08:33:20 am (GMT) which corresponds to 11:33:20 am (IST). In real water management and planning applications, daily rate of ET is interested. The data for daily reference ET (Fig. 8c) obtained from a nearby meteorological station is

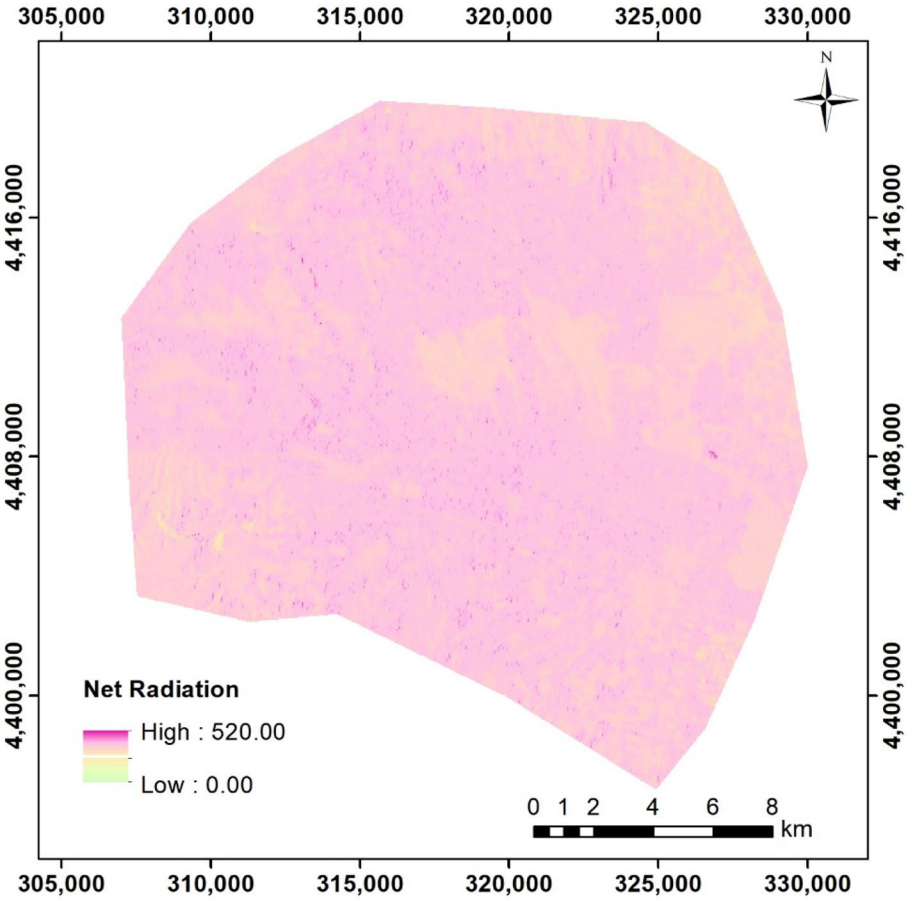

Fig. 6 The map of net radiation ($W.m^{-2}$). It is calculated by subtracting all leaving radiation terms from incoming radiation according to Eq. (3)

used to extrapolate the instantaneous ET data to every hour of the day. For example at 11:33:20 am (IST) which is the acquisition time, the ET_r was recorded as 0.5 mm (Fig. 8b). For a later time at 15:00:00 it was 0.6 mm. Therefore, to obtain the ET for each pixel at 15:00:00, the instant ET for each pixel on the map must be multiplied by 0.6/0.5. The same approach when applied for every hour of the day and then their summation provides 24 hour or daily ET estimation over the study area as presented in Fig. 8c. The interesting observation is that the instant ET map which can be assumed as a specific hour ET data is estimated to vary between 0 to 0.5 mm (Fig. 8a). The meteorological data also shows 0.5 mm which is close the highest ET estimations on the map. This also supports accuracy of the method. The 24 h ET data on map in Fig. 8c shows that the range of ET was between 0 to 9 mm per day over the region. It was observed that the obtained map is adequately informative even at farm scale like for two adjacent

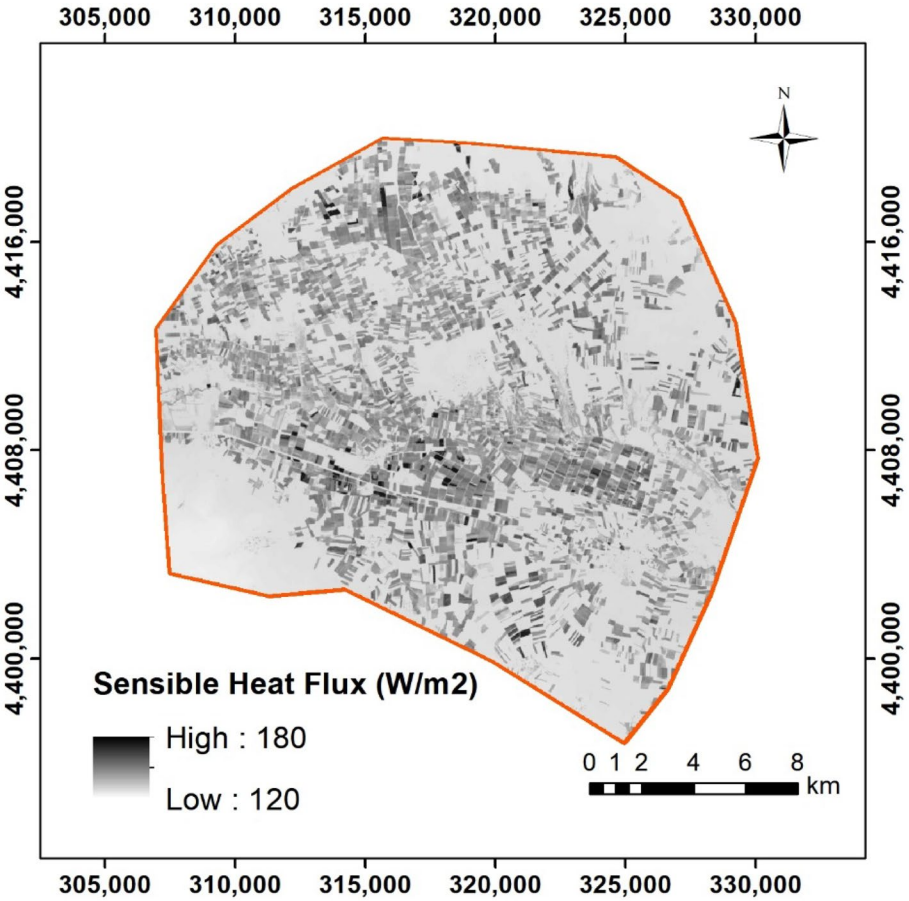

Fig. 7 Sensible heat flux H (W/m^2) over the study area. Sensible heat flux is the amount of energy being transferred from land surface to the atmosphere

farms with 1 or 2 ha land area. Comparing the ET map in Fig. 8c with the RGB image of the study area in Fig. 1 also reveals high resolution of ET map with significant contrast.

As a comparison, in a study also using METRIC model over a single 50 ha alfalfa farm in Saudi Arabia for different days between June to October where in the range of 0.09-0.86 mm/h (Madugundu et al. 2017). Daily ET over large region of olive orchard with drip-irrigation in Chile for different days of the year between 2012-2013 was estimated in the range of 4.4-7.7 mm/d (Ortega-Salazar et al. 2021).

METRIC model can also be used to estimate ET over longer time span like monthly, seasonal or even yearly basis where the vegetation type does not change so frequently like prairie or wetlands as was reported in (Baeumler et al. 2019).

3.2 Evaluation of Model Output for Small Farms

While above output maps are showing general overview of the region ET behavior, for more specific needs like water management on farm scale, additional explanations over a focused area is provided here. In Fig. 9, for an area of about 1110 ha, major factors map are presented. The area includes range of approximate 2 to 80 ha farms, with various type of vegetation. At this point, the results show that for some factors like NDVI, albedo and surface emissivity the boundary of farms are clear so that an almost uniform value was estimated for a single farm. These are factors which are directly calculated from spatial data which has high resolution. It means any reduction in the specificity of the data for a farm might have come from other sources like primary effect of meteorological factors which does not change meaningfully for two adjacent farm.

For LST, larger farms or non-cultivated large farms are distinguishable but the smaller ones are faded on the LST map. It can be explained by governing Eqs. (22), (23), (24), (25), (26) and (27). The split window algorithm actually has three main components including top of atmosphere brightness temperature (T_B), emissivity (ε) and water content (W). In calculation procedure for T_B and ε , there are parameters which are either constants or depends linearly on spatial pixel value which makes them uniform over a specific farm. In contrast, W is calculated from meteorological data and then distributed based on elevation. Therefore, since it is not directly related to spatial data, the variation over adjacent farms are smooth where farms boundary are faded. This scheme actually is in consistent with physics of the phenomenon where water content over an area is homogenized by air movements and buoyancies. Other water content estimation methods which are based on spatial data may improve the quality of LST map but there are significant biases in those models (Jiménez-Muñoz and Sobrino 2005).

Among the major energy terms in Eq. (1) (Fig. 9), sensible heat transfer map has farm specific estimations but for the other radiation terms, they are more or less insensitive in farm scale. The long wave output radiation (R_{Lo}) is still farm specific to some extent but not as specific as sensible heat (H) term. This is not specific to METRIC model since incoming short-wave radiation and incoming-long-wave radiation in all remote sensing based ET models are calculated from Boltzmann equation (Eqs. 21 and 30) which is dependent on the temperature of the sources other than land surface. As can be seen from Fig. 9, the effect of R_{Li} is not significant because for the selected zoon, the maximum and minimum values are very close to each other with less than 0.05% variations. The main reason for changing shortwave radiation over a farm is the topography, where the variation in the aspect from southeast to northwest for the acquisition time, the amount of received radiation substantially changes. Therefore, the observed non-homogeneous distribution (i. e. not farm specific) for incoming shortwave radiation (Fig. 9) is normal. This term of energy for the selected zoon varies between 570-785 W/m^2 which is the most determining term of energy. The faded boundary of the farms in net radiation (R_n) and consequently the ET map is therefore expectable. To estimate ET over a specific farm, user can make a summation of every pixel value.

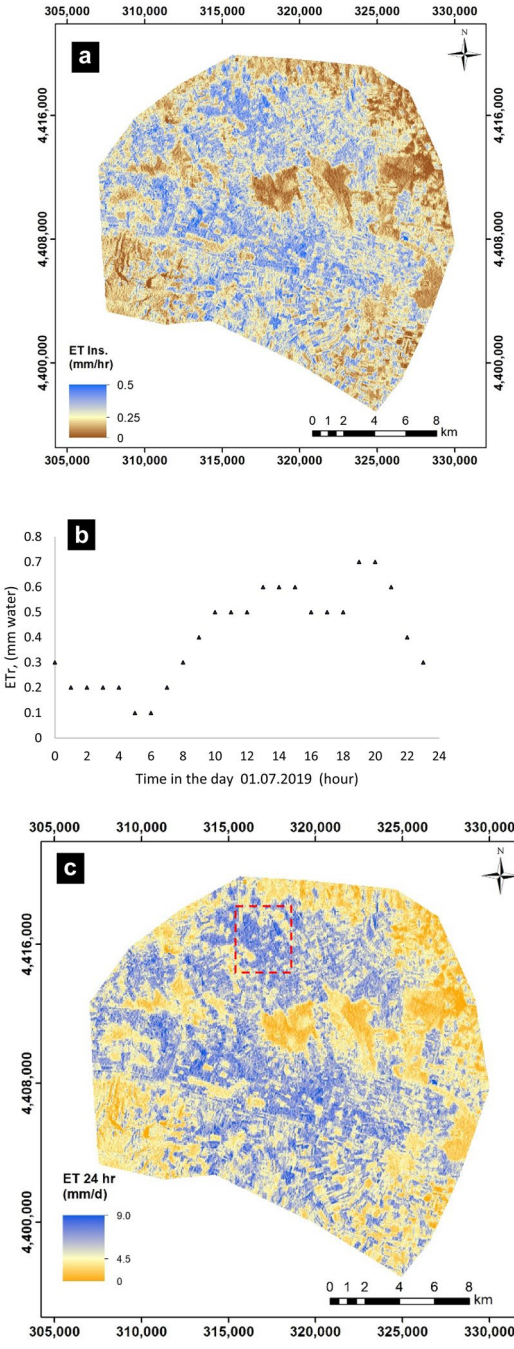

Fig. 8 **a**) Instant Evapotranspiration rate (mm/hr). The result of all the calculations finally when applied in Eq. (62) gives the ET rate at the acquisition time of the image. **b**) Meteorological data for reference ET from a nearby station. **c**) 24 hour Evapotranspiration rate (mm/d) over the study area. ET rate for every hour of the day where the imagery data is not available is estimated using the ratio of the instant ET to the reference ET_r data obtained from nearby local meteorological stations. Specified area inside red rectangle is magnified in Fig. 9 for more explanations

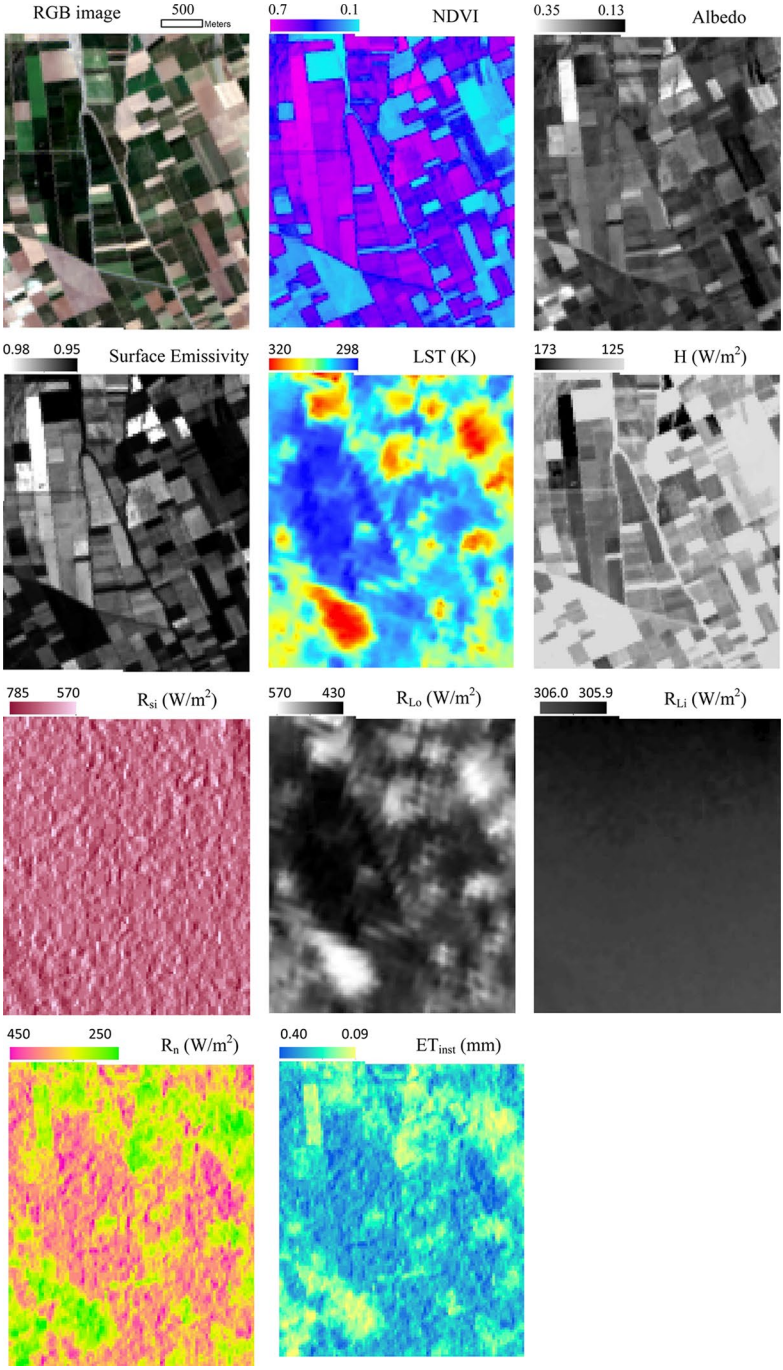

Fig. 9 The magnified image of specified red recrangle in Fig. 8 for various factors including RGB image, NDVI index, albedo factor, surface emissivity, LST, H (W/m^2), R_{si} (W/m^2), R_{Lo} (W/m^2), R_{Li} (W/m^2), R_n (W/m^2) which influence the last obtained ET map. It shows clear boundaries of farms in final ET map which means it can be used to obtain ET estimations for even small farms

4 Conclusion

In this study, METRIC model was applied to estimate evapotranspiration over intensively irrigated agriculture land in a small region. It was concluded that METRIC approach is a useful effective method for estimations of evapotranspiration when calibrated for high resolution imagery spatial data from Landsat 8. The results of this study show that evaporation rates between 0-0.5 $mm.h^{-1}$ was estimated based on the data from spatial satellite imagery at capture time. The ET map over the study area clearly shows that the active irrigated farms have significant evapotranspiration rate when compared to bare or settlement land covers. It was ranging up to 9 mm per square meter in 24 hours. The Landsat 8 platform provides high resolution multispectral images where makes it possible to apply METRIC models to even small farms so that the water management policies could be applied more effectively.

Acknowledgment This project was funded by Eskişehir Technical University under project No. 19ADP056.

Data Availability Authors agree with data transparency and undertake to provide any required data and material.

Code Availability Authors agree with code transparency and undertake to provide any required material.

Declarations

Ethics Approval Not applicable.

Consent to Participate Not applicable.

Consent for Publication Not applicable.

Competing Interests The authors declare no competing interests.

References

Allen RG, Tasumi M, Trezza R (2007) Satellite-based energy balance for mapping evapotranspiration with internalized calibration (METRIC)—Model. J Irrig Drain Eng 133(4):380–394

Baeumler NW, Kjaersgaard J, Gupta SC (2019) Evapotranspiration from corn, soybean, and prairie grasses using the METRIC model. Argon J 111(2):770–780

Bastiaanssen WG (2000) SEBAL-based sensible and latent heat fluxes in the irrigated Gediz Basin, Turkey. J Hydrol 229(1–2):87–100

Bastiaanssen WG, Sakthivadivel R, Van Dellen A (1999) Spatially delineating actual and relative evapotranspiration from remote sensing to assist spatial modeling of non-point source pollutants. GMS 108:179–196

Bastiaanssen WGM (1995) Regionalization of surface flux densities and moisture indicators in composite terrain: A remote sensing approach under clear skies in Mediterranean climates, SC-DLO

Faivre R, Colin J, Menenti M (2017) Evaluation of methods for aerodynamic roughness length retrieval from very high-resolution imaging lidar observations over the Heihe Basin in China. Remote Sens 9(1):63

Garrison JD, Adler GP (1990) Estimation of precipitable water over the United States for application to the division of solar radiation into its direct and diffuse components. Sol Energy 44(4):225–241

Huang D, Wang J, Khayatnezhad M (2021) Estimation of actual evapotranspiration using soil moisture balance and remote sensing. Iran J Sci Technol Trans Civil Eng 1–8

Huete AR (1988) A soil-adjusted vegetation index (SAVI). Remote Sens Environ 25(3):295–309

Jiménez-Muñoz JC, Sobrino JA (2005) Atmospheric water vapour content retrieval from visible and thermal data in the framework of the DAISEX campaigns. Int J Remote Sens 26(15):3163–3180
Jin M, Li J, Wang C, Shang R (2015) A practical split-window algorithm for retrieving land surface temperature from Landsat-8 data and a case study of an urban area in China. Remote Sens 7(4):4371–4390
Li S, Zhao W (2010) Satellite-based actual evapotranspiration estimation in the middle reach of the Heihe River Basin using the SEBAL method. Hydrol Process 24(23):3337–3344
Li Z-L, Wu H, Wang N, Qiu S, Sobrino JA, Wan Z, Tang B-H, Yan G (2013) Land surface emissivity retrieval from satellite data. Int J Remote Sens 34(9–10):3084–3127
Lian J, Huang M (2015) Evapotranspiration estimation for an Oasis Area in the Heihe River Basin Using Landsat-8 Images and the METRIC model. Water Resour Manag 29(14):5157–5170
Liang S (2001) Narrowband to broadband conversions of land surface albedo I: Algorithms. Remote Sens Environ 76(2):213–238
Liang S, Strahler AH, Walthall C (1999) Retrieval of land surface albedo from satellite observations: a simulation study. J Appl Meteorol 38(6):712–725
Madugundu R, Al-Gaadi KA, Tola E, Hassaballa AA, Patil VC (2017) Performance of the METRIC model in estimating evapotranspiration fluxes over an irrigated field in Saudi Arabia using Landsat-8 images. Hydrol Earth Syst Sci 21(12):6135
Ortega-Salazar S, Ortega-Farías S, Kilic A, Allen R (2021) Performance of the METRIC model for mapping energy balance components and actual evapotranspiration over a superintensive drip-irrigated olive orchard. Agric Water Manag 251:106861
Paredes P, Pereira LS (2019) Computing FAO56 reference grass evapotranspiration PM-ETo from temperature with focus on solar radiation. Agric Water Manag 215:86–102
Sissenwine N, Dubin M, Wexler H (1962) The US standard atmosphere, 1962. J Geophys Res 67(9):3627–13630
Smith RB (2010) The heat budget of the earth's surface deduced from space. Yale University Center for Earth Observation: New Haven, CT, USA
Sobrino J, El Kharraz J, Li Z-L (2003) Surface temperature and water vapour retrieval from MODIS data. Int J Remote Sens 24(24):5161–5182
Sun Z, Wei B, Su W, Shen W, Wang C, You D, Liu Z (2011) Evapotranspiration estimation based on the SEBAL model in the Nansi Lake Wetland of China. Math Comput Model 54(3–4):1086–1092
Tasumi M (2004) Progress in operational estimation of regional evapotranspiration using satellite imagery
Walter IA, Allen RG, Elliott R, Jensen M, Itenfisu D, Mecham B, Howell T, Snyder R, Brown P, Echings S (2000) ASCE's standardized reference evapotranspiration equation. Watershed Manag Oper Manag 2000:1–11
Xiang K, Li, Y, Horton R, Feng H (2020) Similarity and difference of potential evapotranspiration and reference crop evapotranspiration – a review. Agric Water Manag 232:106043
Zhao L, Xia J, Xu C-Y, Wang Z, Sobkowiak L, Long C (2013) Evapotranspiration estimation methods in hydrological models. J Geogr Sci 23(2):359–369